The Canadian Mineralogist
Vol. 36, pp. 265-282 (1998)

THE RICHEMONT RHYOLITE DYKE, MASSIF CENTRAL, FRANCE: A SUBVOLCANIC EQUIVALENT OF RARE-METAL GRANITES*

LOUIS RAIMBAULT[1]

Centre d'Informatique Géologique, Ecole des Mines, 35, rue St Honoré, F-77305 Fontainebleau Cedex, France et Groupe des Sciences de la Terre, Laboratoire Pierre Süe, C.E.N. Saclay, B.P. 2, F-91191 Gif-sur-Yvette Cedex, France

LUCIEN BURNOL†

62, rue A. Joly, F-78000 Versailles, France

Abstract

A rhyolitic dyke at Richemont, Haute-Vienne, France, is shown to be the subvolcanic counterpart of rare-metal-bearing granites and pegmatites. Textural relationships provide evidence for a quenched silicate melt with less than 5% phenocrysts, consisting of albite (50%), quartz (20%), K-feldspar (20%), and muscovite (10%). The affinity with pegmatites arises from the ore mineralogy, with "uran-euxenite" and "wolframo-ixiolite" as the main rare-metal carriers. An affinity with rare-metal granites arises from the geochemistry. The composition of the rhyolite is quite similar to that of the Beauvoir Ta–Li-bearing granite, corresponding to the high-phosphorus, high-fluorine class of strongly peraluminous leucogranites, enriched in Ta, Nb, Sn, Li, and Be. The melt belongs to the family that typically crystallizes as LCT granitic pegmatites. Analyses of muscovite phenocrysts provide estimates of muscovite – melt partition coefficients, allowing an explanation of some geochemical characteristics of this type of magmatism, *e.g.*, Li, Cs, Ta and Sn increase during differentiation, and patterns of fractionation involve the ore elements W, Nb and Ta. Isolated aggregates of phosphate with inclusions of sulfosalts and of Nb, W, and Sn oxides are interpreted as signaling the onset of silicate – phosphate melt unmixing processes. Microcrystalline facies of the rhyolite are tentatively identified as the result of complete fluid unmixing, allowing a qualitative assessment of element extraction by fluids escaping from high-F melts. Although Sn, Ti, Th, Nb, and Ta are not depleted relative to the melt, other elements are removed, mildly in the case of Rb, Mn, S, Be, and Zn, strongly in the case of U, Li, B, As, F, and Ba, and very strongly in the case of W, Sb, Sr, P, and Ca.

Keywords: rhyolite, rare-metal-enriched melt, pegmatite-forming melt, magmatic differentiation, Nb–Ta oxide, muscovite, partition coefficient, Richemont, Haute-Vienne, France.

Sommaire

Le dyke rhyolitique de Richemont (Haute-Vienne, France) est un équivalent subvolcanique des granites et pegmatites à métaux rares. Les relations texturales montrent qu'il s'agit d'un liquide silicaté trempé comportant moins de 5% de phénocristaux, formés d'albite (50%), de quartz (20%), de feldspath potassique (20%) et de muscovite (10%). L'affinité avec les pegmatites relève de la minéralogie, les principaux minéraux porteurs de métaux rares étant les espèces "uran-euxénite" et "wolframo-ixiolite". L'affinité avec les granites relève de la géochimie, la composition de la rhyolite étant tout à fait similaire à celle du granite de Beauvoir minéralisé en Ta–Li, et correspond à la classe des leucogranites très peralumineux riches en phosphore et fluor et enrichis en Ta, Nb, Sn, Li et Be. Le liquide appartient au groupe qui cristallise normalement sous forme de pegmatites granitiques de type LCT. La détermination des coefficients de partage muscovite – liquide permet d'expliquer certaines caractéristiques géochimiques de ce type de magmatisme, par exemple l'augmentation de Li, Cs, Ta et Sn au cours de la différenciation, ou le fractionnement impliquant les éléments W, Nb et Ta. Des aggrégats de phosphates isolés, avec des inclusions de sulfosels et d'oxydes de Nb, W et Sn, représenteraient le début de processus de démixion. Les faciès cristallisés de la rhyolite résulteraient du départ complet de la phase fluide, ce qui permet une évaluation qualitative de l'extraction des éléments par les fluides s'échappant des magmas riches en fluor. Alors que Sn, Ti, Th, Nb et Ta ne sont pas appauvris par rapport au liquide, Rb, Mn, S, Be et Zn sont légèrement emportés, U, Li, B, As, F et Ba sont fortement appauvris, et W, Sb, Sr, P et Ca sont très fortement appauvris.

Mots-clés: rhyolite, magma enrichi en métaux rares, magma formateur de pegmatite, différenciation magmatique, oxyde de Nb–Ta, muscovite, coefficient de partage, Richemont, Haute-Vienne, France.

[1] *E-mail address*: raimbault@cig.ensmp.fr

† Lucien Burnol died on January 1st, 1995.

* GéoFrance-3d contribution number 24.

INTRODUCTION

The Richemont dyke in the northwestern part of the Massif Central, in France, consists of a single batch of a highly evolved, rare-metal-bearing silicate melt. This occurrence belongs to a narrow belt of Li–Ta-bearing magmatic rocks running through 150 km in the northern Massif Central and including, from the east to the west, the Beauvoir and the Montebras granites, the Chèdeville pegmatite field, and the Richemont dyke. The similarity in composition of the primary melts has been noticed since the first comprehensive studies of these occurrences (Burnol 1974, Aubert 1969), and recent dating by the $^{40}Ar/^{39}Ar$ method indicates overlapping ages for Beauvoir and Chèdeville occurrences at 308 Ma (Cheilletz *et al.* 1992) and Montebras at 310 Ma (M. Cuney, private commun.). The chemical composition of the Richemont rocks is similar to one of the facies of the Beauvoir granite (Raimbault & Azencott 1987, Raimbault *et al.* 1995), including trace-element contents and oxygen isotope ratio. However, mineralogical compositions are strikingly different one from the other. The study of this dyke may therefore provide specific information on the magmatic stage of such rocks that cannot be obtained from the study of rare-metal granites *sensu stricto*.

High-silica extrusive rocks corresponding in composition to pegmatite-forming magmas have been recently described from Honeycomb Hills, Utah (Congdon & Nash 1991) and from Brockman, Western Australia (Ramsden *et al.* 1993). The Richemont occurrence shares many characteristics with these rocks. Notable also is its similarity with granitic pegmatites, as evidenced by a suite of unusual accessory minerals. The Richemont rhyolite is of particular interest owing to its geochemical and mineralogical characteristics relating it to the LCT (for Li–Cs–Ta) class, whereas the Honeycomb Hill rhyolites and Brockman volcanic suites belong to the NYF (for Nb–Y–F) pegmatite class of Černý (1992).

GEOLOGICAL SETTING

The Richemont rare-metal rhyolite occurs as a 5-km-long dyke on the northern side of the Blond granite massif (Fig. 1). The dyke intrudes a Devonian metamorphic complex consisting of amphibolites identified by their geochemistry as meta-andesites, and gneisses derived from biotite granites. The Blond granite consists of two-mica granite and is spatially associated with numerous small tungsten–tin deposits, now depleted. A late Carboniferous age of 314 ± 5 Ma has been obtained by the Rb–Sr method (Duthou 1977). Both the Blond granite and the Richemont rhyolite were emplaced at a high level in the crust.

Outcrop conditions are poor, and the dyke geometry is known chiefly owing to some small quarries and to short drillholes. Although the dyke is continuous for more than 5 km, its width does not exceed 6 meters. The typical facies, hereafter referred to as the rhyolitic facies, has been defined in a small quarry near the Richemont farmhouse: small phenocryts (less than 2 mm in size) can be identified in an aphanitic groundmass. Banded textures, defining the banded facies, are present near the contact with surrounding rocks. Spaces between bands are approximately 1–2 mm wide, and becomes larger toward the central part of the vein, where such textures are occasionally found. At some distance from this quarry, and in many places along the dyke, the aspect of the rock is remarkably similar, except that the groundmass appears as an aplite-like fine-grained granitic rock. The latter facies is hereafter referred to as the microcrystalline facies.

ANALYTICAL METHODS

Analytical methods used for whole-rock analyses include X-ray-fluorescence spectrometry (XRF) for SiO_2, Al_2O_3, CaO, K_2O, P_2O_5, Ga, Sr, Zr, Nb, Sn, Ba, and Pb (J.J. Gruffat, Y. Baud and C. David, analysts), instrumental epithermal (IENAA) and thermal (ITNAA) neutron-activation analysis for As, Br, Rb, Mo, Ag, Sb, Cs, Ta, W, U, and Na_2O, Sc, Mn, Fe^{total}, Co, Zn, Hf, and Th, respectively (L. Raimbault, analyst), radiochemical neutron-activation analysis (RTNAA) for the rare-earth elements (*REE*) La to Lu (L. Raimbault and J.L. Joron, analysts), inductively coupled plasma – atomic emission spectrometry (ICP–AES) for Li, Be, Mg, Ti (J. Moutte and L. Raimbault, analysts), selective-ion electrode (SIE) for F (C. Richard, analyst), atomic absorption spectrometry (AAS) for Cd, and colorimetry for B, S, Cl (M. Vernet and L. Marin, analysts). XRF and ICP–AES analyses were performed at the Geological Laboratory, Ecole des Mines de Saint-Etienne, NAA, at Laboratoire Pierre Süe, C.E.N. Saclay, SIE at Université Paris VI, and AAS at CRPG, Nancy.

Electron-microprobe analyses of minerals were performed using the Camebax instrument at the Ecole des Mines de Paris in Fontainebleau, with standard ZAF correction procedures. Pure oxides and silicates were used as standards for most elements; pure metals were used for Nb and Ta. Mineral separates of phenocrysts were obtained by selective grinding and hand-picking under the binocular microscope. Oxygen isotope analyses were done at BRGM, Orléans (A.M. Fouillac, analyst). Muscovite crystals were analyzed individually by IENAA or as a bulk fraction by ICP–AES. Modal analyses were made by point counting thin sections (2500–3000 points).

PETROGRAPHY

Phenocryst abundance in the rhyolitic facies is low, in the range of 4–5% by volume (Table 1). Phenocryst assemblage includes albite (49–56%), quartz (18–20%),

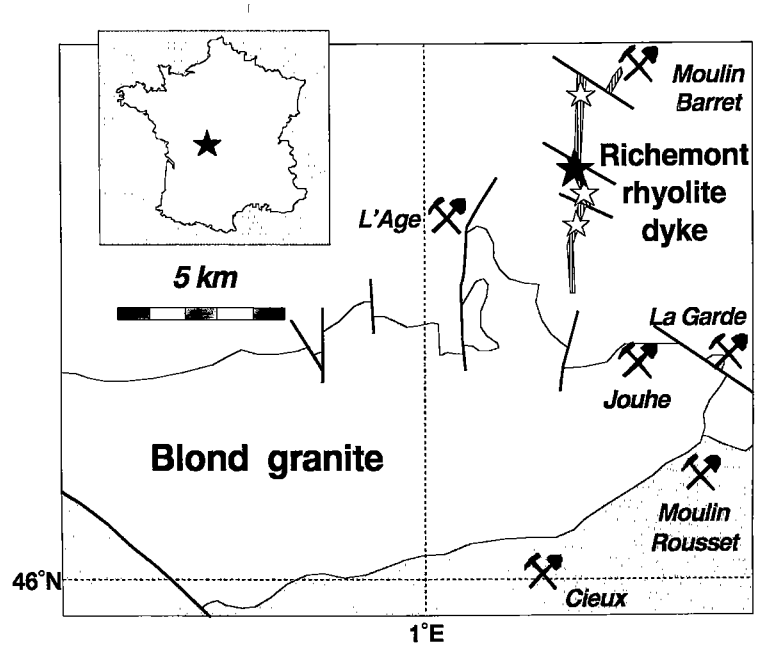

FIG. 1. Geological sketch-map of the Monts de Blond, Haute-Vienne, France. White: metamorphic rocks, light gray: biotite granites, dark gray: Blond two-mica granite, ruled: Richemont rhyolite (the width of the dyke is exaggerated for clarity), filled star: location of the type locality of the dyke, gray stars: other sampling localities. Closed W–Sn mines and prospects also are shown.

K-feldspar (15–22%), and muscovite (10–11%). As a rule, crystal size is smaller than 1 mm (mean size, 0.6 mm), with a few elongate albite crystals up to 2 mm long. Phenocrysts can be found either as isolated, perfectly euhedral crystals, or as aggregates of two to five coprecipitated individuals, each of which tends to develop euhedral faces. Muscovite crystals develop perfect diamond-shaped (001) faces (Fig. 2b). Euhedral inclusions of feldspars and muscovite in feldspar and quartz (Fig. 2a) and of feldspars in muscovite are common. No anhedral crystals or crystals with an anhedral core can be found, suggesting that no xenocrysts are present. Microphenocrysts of niobates occur either as inclusions in or overgrowths on muscovite phenocrysts (Fig. 2b), or as isolated crystals. In both cases, crystals are euhedral, with a lath- or sheet-like habit. The marginal banded facies is characterized by a higher abundance and a slightly different distribution of phenocrysts (Table 1), but with similar mutual relationships.

Sparse rounded aggregates of phosphate crystals are located adjacent to muscovite from phenocryst assemblages, resembling bubbles nucleated at edges of crystals (Fig. 3). Contacts between these aggregates and phenocryst and groundmass are quite sharp and regular, and devoid of any evidence of replacement of

TABLE 1. MODAL ANALYSES OF SELECTED SAMPLES

	L14c3	L14d	L14e1
Groundmass vol.%	95.0	96.0	92.6
Phenocrysts	5.0	4.0	7.4
Aggregates*	0.03	0.04	0.01
Proportion of phenocrysts			
Albite %	56.4	48.7	39.7
K-feldspar	14.8	21.6	30.4
Quartz	18.1	19.8	25.8
Muscovite	10.7	9.9	4.1

* Roundish aggregates of fine-grained anhedral phosphates with inclusions of sulfosalts or oxides.

either phenocrysts by aggregates or aggregates by groundmass. In contrast to usual phosphate textures in granites, apatite crystals are never idiomorphic. Inclusions of ore minerals are dispersed throughout the aggregates. Associations studied include: apatite + high-S löllingite ± W–Nb-oxide ± scheelite, apatite + W–Nb-oxide + löllingite + arsenopyrite ± wolframite, apatite + W–Nb-oxide + wolframite + cassiterite + zircon, and apatite + amblygonite + Na-phosphate +

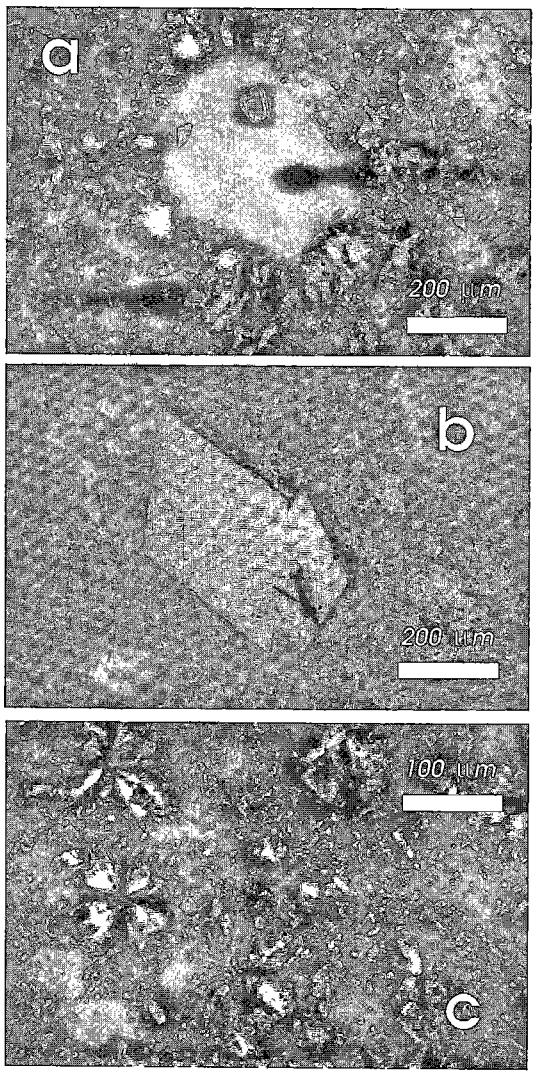

FIG. 2. Thin-section microphotographs, sample L14d, rhyolitic facies. a. Quartz phenocryst (black) with two inclusions of euhedral muscovite (polarized light). The aureole around the quartz phenocryst indicates that phenocrysts likely acted as nuclei during the process of devitrification. b. Euhedral phenocrysts of muscovite with an inclusion and an overgrowth of "wolframo-ixiolite" (plane-polarized light). c. Rosette-like array of lepidolite in groundmass (cross-polarized light).

triplite + tennantite–tetrahedrite. Such textures are absent in the microcrystalline facies.

In the rhyolitic facies, the crystal size in the groundmass varies around 10–20 µm for quartz and feldspars; mica is lepidolite and is arranged in rosette-like structures (Fig. 2c) up to ca. 150 µm in diameter. The contact between phenocrysts and groundmass is very sharp, and no rim is observed. The interstitial texture is interpreted to result from the devitrification of a previously glassy matrix. Grain size in the microcrystalline facies is much larger, about 80 µm; quartz, feldspar and mica define an aplite-like texture quite identical to the usual textures of such magmatic rocks. Unlike the rhyolitic facies, overgrowth of an albite or muscovite rim around the corresponding phenocrysts is common.

Phenocryst alteration is limited to the development of rare epidote and patchy secondary apatite on albite; the K-feldspar is cloudy, probably the result of microcrystalline kaolinite. Parallel quartz veinlets, about

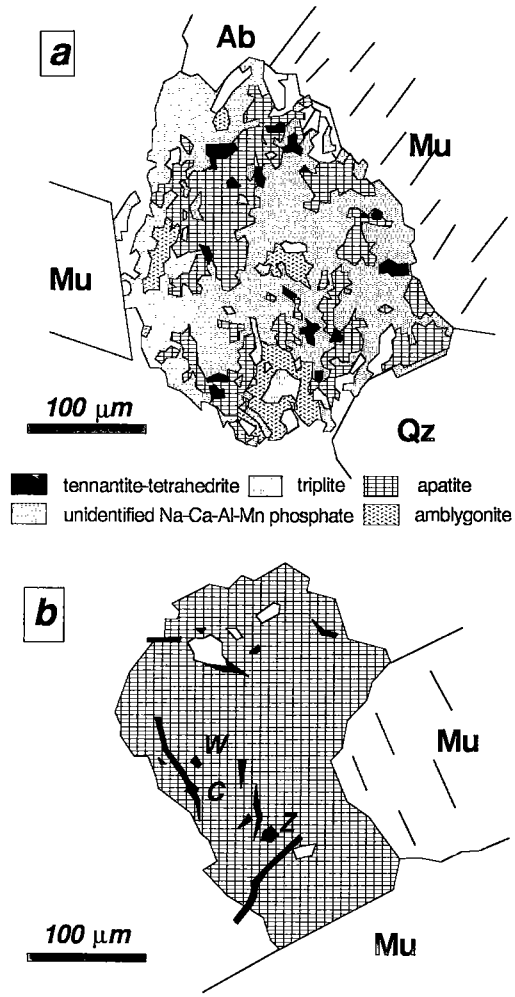

FIG. 3. Phosphate aggregates reconstructed from X-ray images. In white: groundmass and phenocrysts. Symbols: Mu muscovite, Ab albite, Qz quartz.

30 μm wide, cut straight across all textures of the rocks and host some Be minerals (bertrandite has been identified optically, but other very small crystals are present). These veinlets do not induce any alteration and are clearly very late, since they postdate all textures, including those resulting from devitrification. Alteration textures are therefore of quite limited extent and of very low-temperature origin. High-temperature alteration (*e.g.*, leading to greisens, or mineralized quartz-veinlet stockworks), which is usually widespread in high-silica magmatic rocks, is characteristically absent in the Richemont rhyolite. The unusual features of the rhyolitic facies therefore must result from the quenching of a melt.

The occurrence in rhyolites of minerals usually expected in pegmatites has been described at Honeycomb Hills, Utah (Congdon & Nash 1991), and observed in ongonites (topaz-bearing rhyolites) at Ary Bulak, Transbaykalia (Antipin *et al.* 1980, Kovalenko & Kovalenko 1976, Raimbault, unpubl. data). However, topaz is abundant as phenocrysts in these two occurrences, whereas it is absent at Richemont, where fluorine is carried by matrix-hosted lepidolite resulting from the devitrification of glass. The nature of the mica (siderophyllite *versus* muscovite) also discriminates between the two groups. Eruptive pegmatite-forming magmas are rare, but the few observations available indicate different types of pegmatite classes, and suggest a more widespread occurrence than previously expected. Such rocks are of great interest on their own right, but also in the context of pegmatite studies, since they provide insight into the earliest stages of magmatic evolution of pegmatite-forming melts, owing to their phenocryst assemblage.

Mineralogy

Feldspar

The feldspar phenocrysts are albite and K-feldspar, both of nearly pure end-member composition. In albite, the anorthite component remains below 0.1%, and the orthoclase component clusters around 0.5%, with one value at 1.7%. K-feldspar phenocrysts are devoid of visible perthite lamellae, with a very narrow range of albite component from 2.0 to 2.3%. Compositions are uniform over the whole crystals, and even the overgrowth rim around an albite phenocryst from the microcrystalline facies has the same composition as the core.

Muscovite

As muscovite phenocrysts have a rather homogeneous composition (Table 2), the ICP–AES bulk analyses of muscovite separates for Li (see below) are representative of the mean Li contents (0.44% Li_2O). Moreover, the Rb contents of individual crystals vary in a narrow

TABLE 2. COMPOSITION OF MUSCOVITE PHENOCRYSTS, RICHEMONT DYKE, MASSIF CENTRAL, FRANCE

	Ll4d, rhyolitic		Ll4e1, banded		Ll4a, microcrystal	
Anal.#	45	47	55	58	1	4
SiO_2	45.67	44.00	45.31	44.70	45.95	45.17
Al_2O_3	35.22	32.07	35.24	32.43	35.68	34.00
FeO	3.24	6.69	3.05	6.37	2.75	4.59
MnO	0.14	0.24	0.08	0.23	0.05	0.19
TiO_2	0.14	0.18	0.09	0.15	0.07	0.18
K_2O	10.59	10.66	10.60	10.67	10.27	10.56
Na_2O	0.85	0.63	0.89	0.67	0.92	0.74
F	2.13	2.03	1.58	2.44	1.76	1.27
H_2O^-	3.50	3.38	3.73	3.24	3.69	3.85
$-O\equiv F$	-0.90	-0.85	-0.67	-1.03	-0.74	-0.53
Total	100.58	99.03	99.90	99.87	100.40	100.02
Si	6.073	6.073	6.059	6.103	6.087	6.082
$^{[4]}$Al	1.927	1.927	1.941	1.897	1.913	1.918
$^{[6]}$Al	3.594	3.291	3.614	3.321	3.658	3.478
Fe	0.360	0.772	0.341	0.727	0.305	0.517
Mn	0.016	0.028	0.009	0.027	0.006	0.022
Ti	0.014	0.019	0.009	0.015	0.007	0.018
Sum oct:	4.199	4.325	4.189	4.306	4.190	4.251
K	1.797	1.877	1.808	1.858	1.735	1.814
Na	0.219	0.169	0.231	0.177	0.236	0.193
Sum int:	2.048	2.078	2.072	2.068	2.004	2.040
F	0.896	0.886	0.668	1.054	0.737	0.541
OH^-	3.104	3.114	3.332	2.946	3.263	3.459

Electron-microprobe data, in weight %. Structural formulas were recalculated on the basis of 24 atoms of oxygen. In addition to the above, 0.195 *apfu* (atoms per formula unit) of Li, 0.014 of Mg, 0.006 of Zn and 0.032 of Rb are estimated from the analysis of mineral separates. The proportion of OH and H_2O are calculated from stoichiometry constraints. Detection limit for CaO and Cl: 0.02%.

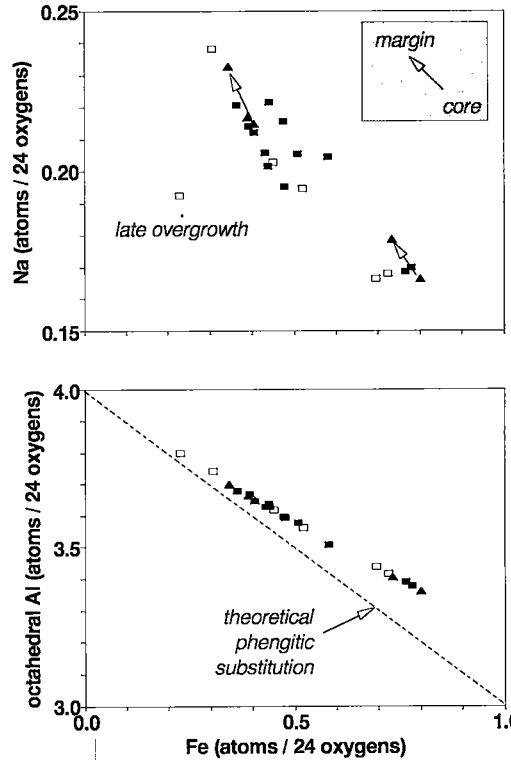

FIG. 4. Correlation between amount of Na or $^{[6]}$Al, and Fe in muscovite phenocrysts. Filled rectangles: rhyolitic facies, open rectangles: microcrystalline facies, triangles: banded facies. The label "late overgrowth" indicates a thin rim around phenocryts of the microcrystalline facies.

range from 0.42 to 0.51% Rb_2O. This can therefore be defined as Li-, Rb- and F-rich muscovite. Magmatic muscovite, although slightly less F- and Li-rich than at Richemont, has been described in rhyolites from Germany (Schleicher & Lippolt 1981). The irrelevance of the occurrence of magmatic muscovite as an indicator of magmatic pressure has also been advocated by Dubray (1994). Some differentiation within the muscovite-phenocryst population is evidenced by correlations among Fe, $^{[6]}$Al and Na (Fig. 4). Regardless of the rock facies, compositions cluster into two groups (in one case, a muscovite rim from the microcrystalline facies falls outside the two groups, indicating a two-stage history for this facies.) Of the two groups, one is

TABLE 3. REPRESENTATIVE COMPOSITIONS OF PHOSPHATES AND ZIRCON FROM AGGREGATES, RICHEMONT DYKE, MASSIF CENTRAL, FRANCE

parag.	S	A	O	S	S	S	S	O	O
species		apatite		M	T	NCAM		zircon	
Anal.#	1346	1354	1357	1349	1361	1348	1353	1385	1386
P_2O_5	42.13	41.55	41.26	49.72	33.76	30.85	33.05	1.38	3.84
SiO_2	0.04	0.06	0.05	0.19	0.07	0.05	0.28	27.71	27.63
Al_2O_3	0.06	0.04	0.03	36.97	0.11	22.70	29.12	0.07	0.86
CaO	52.10	50.64	47.29	0.10	2.45	13.84	18.73	1.15	2.81
MnO	3.64	3.92	5.40	1.17	51.95	18.70	10.88		
FeO	–	–	2.02	0.10	5.91	0.54	0.20	0.25	0.76
Ce_2O_3	–	–	0.23	–	–	–	–		
Y_2O_3	–	–	0.50	–	–	–	–	0.93	1.63
UO_2	–	0.84	–	–	–	–	–	2.54	3.95
ZrO_2								53.78	52.81
HfO_2								4.67	4.18
TiO_2									0.18
Na_2O	–	0.06	0.20	0.15	–	9.70	5.59		
F	3.85	3.49	4.08	4.14	6.97				
–O=F	–1.62	–1.47	–1.72	–1.74	–2.93				
Total	100.20	99.13	99.34	90.80	98.29	96.38	97.85	92.48	98.65
P	3.007	3.009	3.009	0.978	1.043			0.040	0.103
Si	0.003	0.005	0.004	0.004	0.003			0.948	0.879
Al	0.006	0.004	0.003	1.012	0.005			0.003	0.032
Ca	4.707	4.641	4.364	0.003	0.096			0.042	0.096
Mn	0.260	0.284	0.394	0.023	1.605				
Fe			0.146	0.002	0.180			0.007	0.020
Ce			0.007						
Y			0.023					0.017	0.028
U		0.016						0.019	0.028
Zr								0.897	0.819
Hf								0.046	0.038
Ti									0.004
Na		0.010	0.033	0.007					
F	1.027	0.944	1.111	0.304	0.804				

Electron-microprobe data, quoted in weight %. Structural formulas, based on the following number of oxygen atoms: apatite 12.5, montebrasite (M) 4, triplite (T) 4.5, zircon 4. NCAM: unidentified Na-Ca-Al-Mn phosphate. *A*: apatite in albite phenocryst, *O*: phosphate aggregate with oxides, *S*: phosphate aggregate with sulfosalts. Limits of detection (dash): FeO 0.05, Ce_2O_3 0.14, Y_2O_3 0.04, Cl 0.02% (phosphates); ThO_2 0.12% (zircon).

characterized by higher Fe and lower Na contents than the second, which also shows more scatter in its analytical data. Although each phenocryst belongs to one group only (*i.e.*, no strong zonation has been observed), a very weak fractionation occurs within phenocrysts (arrows in Fig. 4), suggesting that the Fe-rich group is also the earliest. The Na–Fe correlation is more scattered than the $^{[6]}$Al–Fe correlation. The former corresponds to independent schemes of substitution, and the correlation is likely governed by two different physicochemical conditions of crystallization; in contrast, the well-correlated variations between $^{[6]}$Al and Fe are due to precise crystal-chemical control. The equation of the straight line,

$$^{[6]}Al = {}^{[6]}Al_0 - 0.74 \times Fe,$$

shows that the substitution involves approximately 74% of $Al_{-1}Fe_1$ and 26% of $(Al,Fe)_{-1}Li_1$ substitution.

Phosphate aggregates

To date, four phosphate minerals have been identified in the phosphate aggregates of the rhyolitic facies in the Richemont rhyolite. Apatite is the most common, and it is the only phosphate in most occurrences, where it is more Mn-rich than apatite from complex assemblages (Table 3). In the latter assemblages, apatite is associated with triplite, amblygonite – montebrasite, an unidentified Na–Ca–Al–Mn phosphate, and sulfosalts (see below). The very complex intergrowths show no evidence of replacement textures (Fig. 3), suggesting that the minerals coprecipitated from a P-rich phase. In one apatite aggregate associated with oxides, a U- and Hf-rich zircon grain has been found (Table 3); it is also rich in Y_2O_3, but more P-rich than required by a xenotime-like substitution, suggesting that other types of substitution are involved. The apatite of this aggregate also is Y-rich.

Oxide and sulfide minerals

Ore minerals are present in three different parageneses (Table 4). They occur either as microphenocrysts, as inclusions in phosphate aggregates, or as minute crystals in the groundmass. A uranium niobate occurs only as phenocrysts, whereas wolframite and sulfosalts are present in phosphate aggregates only. Cassiterite also is found in aggregates, but it occurs mainly as small crystals in the groundmass. A complex W–Nb–Ta oxide is the only opaque phase found in all three cases, but its composition is clearly related to the paragenesis to which it belongs (Fig. 5). Finally, a Ta phase is required by mass-balance arguments (Fig. 6), but has not yet been identified.

Electron-microprobe analyses of the U-niobate (Table 4) closely fit a euxenite-like formula $AB_2O_{6.5}$, where *A* is U with lesser amounts of Y, Ce, Ca, Mn, and Fe, and *B* is Nb with lesser amounts of Ta, W, and Ti. The mineral is metamict, but the shape of the crystal (Fig. 7, top) and its brownish color agree better with a euxenite-like mineral than with a cubic pyrochlore-group member; Aurisicchio *et al.* (1993) recently described uranopolycrase, from a granitic pegmatite. It is a mineral of the same family, which also has U as the main *A*-site cation. The phenocryst hosts an inclusion of a W–Nb oxide (Fig. 7, bottom).

The cation-to-oxygen ratio of the complex W–Nb–Ta oxide from the rhyolitic facies approaches 4:8; the analytical results fail to match either a wolframite-type formula AMO_4 or a columbite-type formula AM_2O_6. It is tentatively referred to as

TABLE 4. REPRESENTATIVE COMPOSITIONS (ELECTRON-MICROPROBE DATA) OF OXIDE MINERALS IN THE RHYOLITIC FACIES L14d, RICHEMONT DYKE, MASSIF CENTRAL, FRANCE

	Microphenocrysts						Crystals in phosphate aggregate					minute crystals in groundmass				
	U-niobate			W-ixiolite						wolfr.	cass.	W-ixiolite		cassiterite		
Size*	180x25	30x5@	70x8"	50x12	40x4	92x7	†	†	40x6	7x4	8x8	15x6	10x4	15x10	25x10	20x15
Anal.#	(5 spots)	884	409	413	888	1364	1362	1368	1380	1383	1376	218	408	224	395	398
WO_3	3.87 ± 0.65	37.31	25.63	29.18	34.62	25.78	39.50	42.06	57.37	72.82	2.56	15.65	14.93	6.86	-	1.75
Nb_2O_5	40.10 ± 0.99	31.60	42.79	39.25	36.18	44.51	32.79	31.47	17.92	0.72	3.39	35.76	35.62	1.69	-	3.95
Ta_2O_5	4.34 ± 0.17	3.47	5.85	5.34	4.57	5.99	4.13	4.23	2.71	0.17	0.47	26.13	26.09	1.13	-	4.27
SnO_2		-	-	3.94	0.42	0.35	0.35	0.51	-	0.28	89.15	0.24	-	88.12	99.59	87.64
TiO_2	0.21 ± 0.05	0.76	1.04	0.80	0.87	1.33	0.89	0.83	0.24	0.10	0.19	1.97	2.09			
ZrO_2	0.17 ± 0.02	0.84	0.33	0.35	0.73							0.45	0.30	-	-	0.34
UO_2	41.53 ± 0.89	8.76	-	0.14	-	-	-	-	-	-		1.67	1.37			
ThO_2	0.10 ± 0.04															
Y_2O_3	0.46 ± 0.05															
Ce_2O_3	0.45 ± 0.09															
FeO	0.71 ± 0.20	13.56	17.16	16.03	16.41	17.98	16.74	15.03	3.89	6.52	2.13	2.32	1.99	1.43	0.27	0.86
MnO	1.78 ± 0.31	3.92	4.05	4.30	4.04	4.13	4.72	7.20	17.16	17.70	0.53	11.69	13.26	1.65	-	0.88
CaO	0.28 ± 0.15															
Total	94.00+	100.22	96.85	99.33	97.84	100.07	99.12	101.33	99.29	98.31	98.42	95.88	95.65	100.88	99.86	99.69
W	0.082	0.747	0.466	0.520	0.647	0.452	0.758	0.804	1.245	0.963	0.017	0.279	0.269	0.044		0.011
Nb	1.484	1.104	1.357	1.220	1.179	1.361	1.098	1.050	0.678	0.017	0.038	1.110	1.119	0.019		0.044
Ta	0.097	0.073	0.112	0.100	0.090	0.110	0.083	0.085	0.062	0.002	0.003	0.488	0.493	0.008		0.029
Sn				0.108	0.012	0.009	0.010	0.015		0.006	0.891	0.007		0.869	0.997	0.869
Ti	0.013	0.044	0.055	0.041	0.047	0.068	0.050	0.046	0.015	0.004	0.004	0.102	0.109			
Zr	0.007	0.032	0.011	0.012	0.026							0.015	0.010			0.004
U	0.756	0.151		0.002								0.026	0.021			
Fe	0.049	0.876	1.006	0.921	0.989	1.017	1.037	0.928	0.272	0.278	0.045	0.133	0.116	0.030		0.018
Mn	0.123	0.257	0.241	0.250	0.247	0.237	0.296	0.450	1.217	0.765	0.011	0.680	0.780	0.035	0.006	0.019
others‡	0.061															

Note: Blank = not determined, dash = below detection limit (WO_3: 0.26, Nb_2O_5: 0.11, Ta_2O_5: 0.20, UO_2: 0.11, SnO_2: 0.10, ZrO_2:0.13, and Y_2O_3: 0.06%). Structural formulas on the basis of 6 oxygens (U-niobate), 2 cations in Nb site (W-ixiolite), 4 oxygens (wolframite), and 2 oxygens (cassiterite).

* Estimation of the extreme dimensions, in μm.

@ inclusion in the U-niobate phenocryst. " inclusion in muscovite phenocryst.

‡ includes Ca 0.025, Th 0.002, Y 0.020, and Ce 0.014.

† part of the 92x7-μm crystal (analysis 1364) which is embedded in the phosphate aggregate.

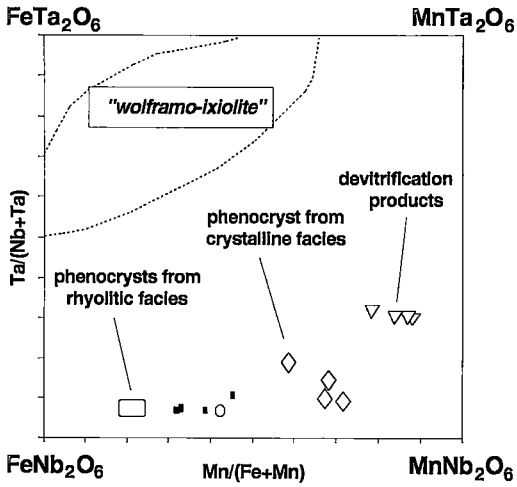

FIG. 5. Projection of the composition of the W–Nb oxides onto the columbite – tantalite quadrilateral (tantalite – tapiolite gap after Černý *et al.* 1992). With one exception (filled circle), phenocrysts from the rhyolitic facies cluster in the shaded area. The small squares refer to oxide grains within phosphate aggregates that do not cluster with phenocrysts. Devitrification products refer to extremely small crystallites (about 10 μm in diameter) dispersed throughout the groundmass.

"wolframo-ixiolite" (Ginzburg *et al.* 1969, Černý & Ercit 1989, Suwimonprecha *et al.* 1995). The systematic presence of Sn, Ti, U also favors this identification. In terms of the columbite – tantalite quadrilateral (Fig. 5), compositions from the rhyolitic facies cluster at $Ta/(Ta + Nb) = X_{Ta} = 0.07$ and $Mn/(Fe + Mn) = X_{Mn} = 0.20$ for microphenocrysts and at $X_{Ta} = 0.31$ and $0.78 < X_{Mn} < 0.88$ for minute crystals in the groundmass. Crystals from apatite aggregates are partly superimposed on the field of compositions of phenocrysts from the rhyolitic facies, but evolve largely toward the manganocolumbite end-member. Similar conclusions arise from the triangular W–Nb–Ta diagram (Fig. 6), with an obvious distinction between phenocrysts and minute crystals, and a link between inclusions in phosphate aggregates and the phenocrysts. However, in this case, there is a clear trend among phenocrysts toward a decrease in tungsten and an increase of Nb and Ta content. The direction of the trend was determined using a grain growing on a muscovite phenocryst (Fig. 2b). Titanium contents increase in correlation with Nb–Ta, and the highest contents are found in the minute crystals. A series of analyses along a crystal astride the contact between the groundmass and an apatite aggregate (Figs. 3, 8) illustrates the transition from phenocrysts occurring in the groundmass to crystals in aggregates. Starting from the phenocryst

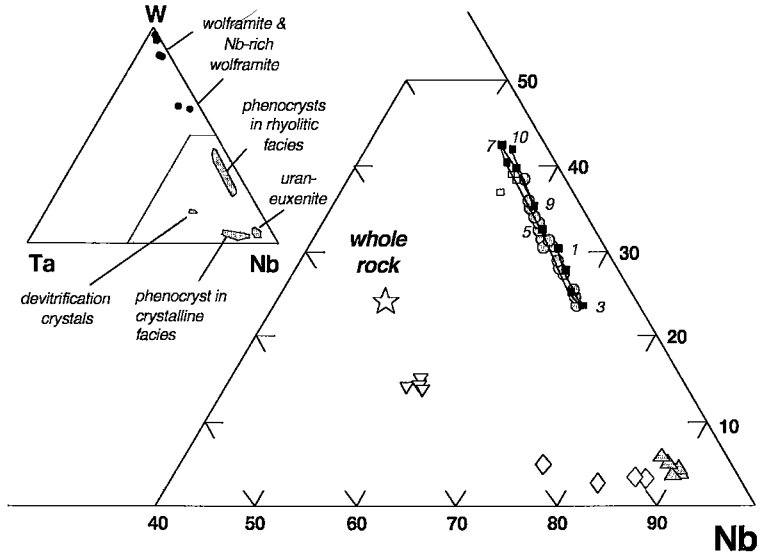

FIG. 6. Atomic proportions of tungsten, niobium, and tantalum in the W–Nb oxide. Gray circles: "wolframo-ixiolite" phenocrysts from rhyolitic facies, inverted triangles: minute "wolframo-ixiolite" crystals from groundmass of rhyolitic facies, diamonds: columbite phenocryst from microcrystalline facies, gray triangles: uranoan euxenite phenocryst, small squares: "wolframo-ixiolite" from phosphate aggregates (black squares labeled 1–10 refer to the phenocryst analyzed in Figure 8, with 1 on the groundmass side and 10 on the aggregate side).

part, a first trend mimics the most evolved part of the phenocryst array (decrease in W, increase of Ta, Nb, Ti contents), followed by a rapid change over *ca.* 10 μm toward a W-rich plateau, with more irregular contents of iron. This leads to very small crystals of true wolframite found in the apatite aggregates. Thus, the crystallization of the phenocryst assemblage seems to have been followed by the formation of the phosphate aggregates, whereas the crystallization of the groundmass appears as a later independent event. Phenocrysts from the microcrystalline facies (Table 5) are somewhat intermediate between phenocrysts of rhyolites and minute crystals, but they characteristically have very low contents of tungsten. Unlike silicate phenocrysts, their composition does not overlap with those of phenocrysts in the rhyolitic facies, suggesting an important episode of re-equilibration.

Total contents of the impurities W, Nb, Ta, and Fe in cassiterite are quite variable, and relative contents of these impurities are strongly scattered. As a result, cassiterite ranges in composition from almost pure SnO_2 to W-, Nb-, or Ta-bearing compositions. This behavior, contrasting with the homogeneous trends of the niobates, suggests that cassiterite did not crystallize at the phenocryst stage, but rather over a large range of physicochemical conditions, from the quenching of the melt down to the latest stage of devitrification. However, the crystal of cassiterite analyzed in the oxide-bearing apatite aggregate has the same W–Ta–Nb proportions as the corresponding "wolframo-ixiolite", suggesting that this stage at least led to uniform compositions.

Sulfosalt-bearing aggregates of phosphates host arsenopyrite, löllingite or tennantite – tetrahedrite crystals (Table 6). Sulfur contents in löllingite are scattered, from high to moderate, and arsenopyrite was found as an overgrowth on löllingite in one case; both are devoid of Sb. On the contrary, the tennantite – tetrahedrite minerals included in the complex phosphate association are intermediate members of the series, with As/(As + Sb) ranging from 0.54 to 0.28; Bi substitutes in variable amounts for As–Sb, copper is in large part replaced by Zn and Cd, which are anticorrelated and, in lesser amounts, by Ag, Pb, and Mn. The concentration of iron is low, ranging from 0.05 to 0.17%.

INTERPRETATION OF MINERALOGICAL DATA

Three distinct stages have been identified, corresponding to the phenocryst assemblage, the phosphate aggregates, and the groundmass, respectively. The compositions of "wolframo-ixiolite" (Figs. 3b, 8) provide evidence of a continuity in crystallization,

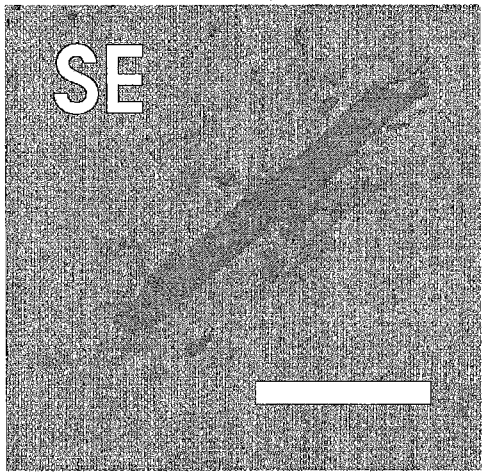

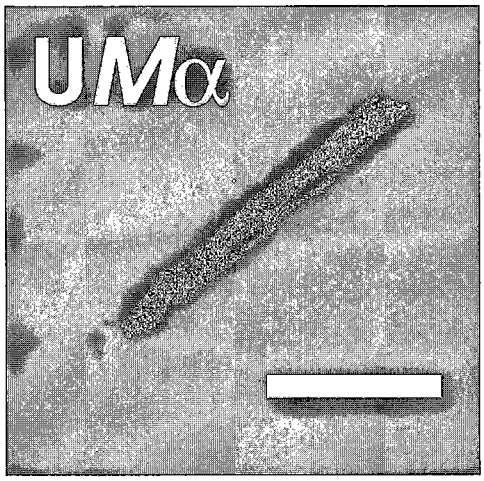

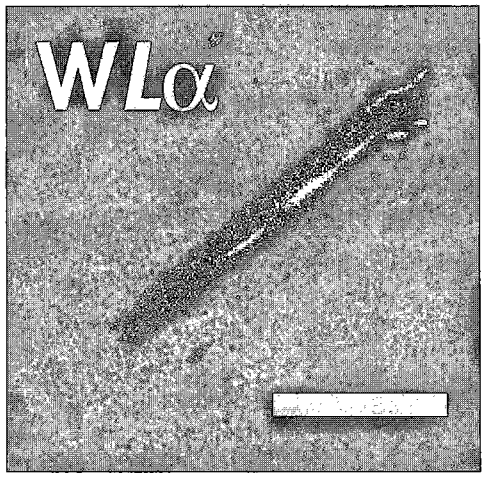

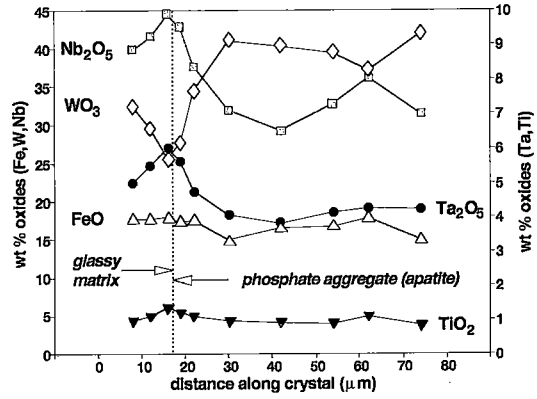

FIG. 8. Variations in composition in the "wolframo-ixiolite" crystal astride the contact between the groundmass and an apatite aggregate (see Fig. 3b). The first three points on the left agree with the overall evolution of the phenocrysts (increase in Nb, Ta, Ti, and decrease in W contents), and are located at the end of the array (Fig. 7); after a short transitional zone, the remaining part correspond to a rather homogeneous W-rich area.

from phenocryst to the onset of phosphate "globule" development; the thin transition-zone within the crystal astride the contact (Fig. 8) can be interpreted as part of the already crystallized ixiolite, which re-equilibrated in the growing phosphate "phase" before quenching of the system as glass phase which later devitrified to give the present groundmass. According to this interpretation, the phosphate aggregates represent the fossil traces of the beginning of a separation process between a silicate melt and a phosphorus-rich phase. However, the physical nature of this phase cannot be inferred unambiguously from our observations. Experiments in fluorine-rich systems have shown large domains of coexistence of silicate and fluoride melts (Gramenitsky & Shchekina 1993). The P-rich phase may have included a fluorine-bearing component, which would account for the low solidus temperature required, and which escaped during quenching. The presence of oxide crystals astride the boundaries of the "globules" suggests that the mineral assemblages are, at least in part, of primary origin.

In addition to petrological evidence, the magmatic origin of the phenocryst assemblage is corroborated by oxygen isotope data (Table 7). Oxygen isotope values for whole rock, quartz, feldspar, and muscovite are

FIG. 7. X-ray images of the uranoan euxenite phenocryst (sample L14d, rhyolitic facies). Scale bar is 50 μm. Top: secondary electron (SE) image; note the halo around the crystal as a result of its highly radioactive character. Middle: U*M*α image. Bottom: W*L*α image. The elongate area, dark in the middle photograph and bright at the bottom, is an inclusion of "wolframo-ixiolite", corresponding to the most primitive composition found in the rock.

TABLE 5. REPRESENTATIVE COMPOSITIONS OF COLUMBITE AND CASSITERITE IN THE MICROCRYSTALLINE FACIES, RICHEMONT DYKE, MASSIF CENTRAL, FRANCE

	columbite		cassiterite				
Anal.#	5322	5324	5124	5125	5128	5130	5131
WO_3	4.38	3.45	0.66	1.69	2.99	0.62	0.80
Nb_2O_5	57.46	53.90	0.52	1.70	9.66	6.24	12.02
Ta_2O_5	11.19	15.51	0.14	0.59	4.47	3.64	7.43
TiO_2	3.07	2.57	0.11	0.30	0.95	0.75	1.12
SnO_2	0.52	0.30	95.43	91.71	74.27	81.00	69.07
UO_2	0.55	0.97					
FeO	6.26	5.81	1.27	1.29	1.45	1.77	2.33
MnO	12.72	12.23	–	0.41	3.55	2.05	3.40
Total	96.15	94.74	98.13	97.69	97.34	96.07	96.17
W	0.070	0.057	0.004	0.011	0.019	0.004	0.005
Nb	1.603	1.557	0.006	0.020	0.108	0.072	0.134
Ta	0.188	0.269	0.001	0.004	0.030	0.025	0.050
Ti	0.142	0.124	0.002	0.006	0.018	0.014	0.021
Sn	0.013	0.014	0.969	0.930	0.730	0.818	0.681
U	0.008	0.008					
Fe	0.323	0.311	0.027	0.027	0.030	0.038	0.048
Mn	0.665	0.662		0.009	0.074	0.044	0.071

Electron-microprobe data, quoted in weight %. Structural formulas are based on six atoms of oxygen (columbite), and two for cassiterite. Blank: not determined, dash: below detection limit (MnO: 0.07%).

granite by Pichavant *et al.* (1987). As commonly observed in granites (*e.g.*, Fouillac & Rossi 1991), the isotopic composition of the feldspars was reset at a lower temperature, and attempts to use the albite–muscovite geothermometer of Green & Usdansky (1986) also yielded low temperatures. The very low contents of albite and orthoclase components in K-feldspar and albite, respectively, seem in contradiction with the results of Stormer (1975), whose experimental determinations of Na partitioning between plagioclase and K-feldspar would suggest a proportion of approximately 20% in K-rich feldspar associated with pure albite at close to 500°C. However, Barton & Frantz (1983) obtained almost pure end-members of the alkali feldspar series in experiments with F-rich fluids. The influence of high f(HF) on feldspar compositions in such systems thus seems to be significant.

TABLE 6. REPRESENTATIVE COMPOSITIONS OF SULFOSALTS, RICHEMONT DYKE, MASSIF CENTRAL, FRANCE

	löllingite			arsenopyrite		tennantite - tetrahedrite			
Anal.#	258	5054	5049	5041	5044	260	264	265	266
Fe	27.63	27.36	27.93	34.54	33.40	0.05	0.09	0.10	0.17
Mn	0.06	–	–	0.08	–	0.28	0.26	0.32	0.61
Cu		–	–	–	0.07	37.94	37.22	37.03	37.35
Zn						6.57	6.65	6.81	6.06
Pb	0.49	0.21	0.19	0.27	0.20	0.36	0.43	0.36	0.31
Ag						0.32	0.43	1.05	0.27
Cd						1.72	1.60	1.32	2.47
As	67.73	67.10	62.40	41.32	45.39	8.85	5.64	6.27	7.71
Sb	–	–	–	0.16	–	12.48	22.10	21.03	15.82
Bi		–	–	–	–	4.25	0.46	0.33	2.75
S	3.06	1.06	5.19	21.51	18.85	26.08	25.49	25.92	25.87
Total	98.97	95.73	95.71	97.88	97.91	98.90	100.37	100.54	99.39
Fe	0.991	1.035	1.003	1.006	1.000	0.02	0.03	0.03	0.05
Mn	0.002			0.002	0.002	0.08	0.08	0.09	0.18
Cu						9.74	9.61	9.47	9.61
Zn						1.64	1.67	1.69	1.52
Pb	0.005	0.002	0.002	0.002	0.002	0.03	0.03	0.03	0.02
Ag						0.05	0.07	0.16	0.04
Cd						0.25	0.23	0.19	0.36
As	1.811	1.893	1.671	0.897	1.013	1.93	1.23	1.36	1.68
Sb				0.002		1.67	2.98	2.81	2.12
Bi						0.33	0.04	0.03	0.22
S	0.191	0.070	0.325	1.091	0.983	13.27	13.04	13.14	13.19

Electron-microprobe data, reported in weight %. Blank: not determined, dash: below limit of detection (Mn: 0.04, Cu: 0.02, Sb: 0.05, Bi: 0.14%. Concentrations of Co and Ni are below the limit of detection (0.03%). Low totals are due to the small size of the crystals. Structural formulas are calculated on the basis of three atoms (löllingite and arsenopyrite) and 29 atoms (tennantite - tetrahedrite).

quite similar to the values found for similar material in the B'2 facies of the Beauvoir rare-metal granite (Fouillac & Rossi 1991). The quartz–muscovite ^{18}O thermometer yields a temperature of 540° ± 50°C using the thermometric curves of Bottinga & Javoy (1975). This estimate is consistent with the low solidus temperatures (560°C) determined for the B'2 Beauvoir

TABLE 7. OXYGEN-ISOTOPE COMPOSITION OF THE RHYOLITIC FACIES, RICHEMONT DYKE, MASSIF CENTRAL, FRANCE

	Whole rock	Quartz	Feldspar	Muscovite
$\delta^{18}O_{SMOW}$ (‰)	+ 9.0	+ 10.6	+ 8.2	+ 7.9

Note: Sample L14c3; analytical precision, ± 0.2 ‰

All the data point out that the rhyolitic facies of the Richemont dyke corresponds to a quenched rare-metal-bearing silicate melt, which underwent very limited re-equilibration at lower temperature. In particular, it seems likely that no loss of the vapor phase occurred, owing to the confined character of the system, which did not erupt. This setting provides an unusual opportunity to evaluate the geochemical characteristics of such melts, including their contents of volatile elements.

Geochemistry of the Rhyolitic Facies

Major elements

The major-element composition of the rhyolite is constant (Table 8), akin to the phosphorus-rich class of rare-metal-bearing melts (Raimbault *et al.* 1991, 1995). It has moderate silica (69.6% SiO_2), high phosphorus and fluorine contents (1.2% P_2O_5, 1.3% F), and is strongly peraluminous, with the atomic ratios Al/(Na + K) and sodic Na/K equal to 1.7 and 1.9, respectively. In terms of the pegmatite classification of Černý (1992), such a peraluminous composition of the melt would have led to a LCT family of pegmatite bodies of the complex type. The distinctly sodic characteristics of the melt are in agreement with the high fluorine contents. The effect of fluorine on the "minimum melt" composition is to displace the eutectic point in the system Qz–Ab–Or–H_2O (Tuttle & Bowen 1958) along a cotectic line in the Qz–Ab–Or–F–H_2O system (Manning 1981). Owing to this effect, residual melts evolve toward the Ab apex with increasing F contents and decreasing solidus temperatures.

As a result of the unusual contents of network-modifier elements (F: Mysen & Virgo 1985; P: Mysen *et al.* 1981a; excess Al: Mysen *et al.* 1981b), the structure of the melt must have been strongly depolymerized, as shown by an estimation of 0.18 for the NBO/T parameter (Mysen *et al.* 1985). A low viscosity of the melt (Dingwell *et al.* 1985) agrees well with the shape of the dyke, which shows a great length for a narrow width. It is otherwise noteworthy that the Richemont rhyolite is geochemically indistinguishable from a related rare-metal granite, the B'2 facies from the Beauvoir complex (Raimbault & Azencott 1987, Raimbault *et al.* 1995). In contrast to the Richemont rhyolite, a differentiation trend occurs in the Beauvoir complex, allowing a comparison of this trend with the characteristics of the Richemont rhyolite.

TABLE 8. MAJOR-ELEMENT COMPOSITION OF THE RICHEMONT DYKE, MASSIF CENTRAL, FRANCE

	rhyolitic facies					banded facies		microcryst. f.	
	L14c1	L14c2	L14c3	L14c4	L14d	L14e1	L14e2	L14b	BL42
SiO_2	69.88	69.34	69.43	69.49	70.00	70.58	70.03	71.76	72.12
Al_2O_3	16.47	16.24	16.35	16.32	16.34	16.34	16.79	16.68	16.47
Fe_2O_3	0.59	0.56	0.59	0.58	0.65	0.60	0.59	0.59	0.54
MnO	0.11	0.11	0.11	0.11	0.11	0.10	0.10	0.09	0.09
CaO	1.21	1.07	1.03	0.65	0.45	1.52	1.16	0.06	0.18
Na_2O	3.43	3.63	3.89	4.12	4.26	3.63	3.70	3.83	4.27
K_2O	3.12	3.08	3.10	3.26	3.04	3.06	3.09	3.59	3.44
Rb_2O	0.21	0.20	0.20	0.21	0.20	0.16	0.17	0.18	0.15
Cs_2O	0.04	0.04	0.03	0.03	0.02	0.04	0.05	0.04	0.03
Li_2O	0.66	0.65	0.66	0.73	0.74	0.46	0.44	0.37	0.30
SnO_2	0.06	0.06	0.06	0.06	0.06	0.07	0.06	0.06	0.06
P_2O_5	1.17	1.17	1.18	1.20	1.16	1.16	0.92	0.10	0.23
H_2O	2.45	2.37	2.15	1.92	1.93	2.13	2.22	1.98	1.32
F	1.25	1.14	1.28	1.22	1.63	0.82	0.88	0.62	0.56
−O≡F	−0.74	−0.68	−0.76	−0.72	−0.97	−0.49	−0.52	−0.37	−0.33
Total	99.91	98.98	99.30	99.18	99.62	100.18	99.68	99.58	99.43

Compositions are reported in weight %.

TABLE 9. TRACE-ELEMENT DATA, RICHEMONT DYKE, MASSIF CENTRAL, FRANCE

	rhyolitic facies					banded facies		microcryst. f.	
	L14c1	L14c2	L14c3	L14c4	L14d	L14e1	L14e2	L14b	BL42
Li	3072	3042	3059	3390	3421	2124	2065	1700	1379
Be	92.1	98.0	99.5	82.5	86.1	64.9	80.0	61.6	58.8
B	68	81	76	69	86	60	51	37	43
Mg	136	81	59	52	45	734	575	420	227
S	130	130	120	130	120	100	120	90	95
Cl	16	12	< 10	< 10	< 10	16	17	33	31
Sc (ppb)	26	19	21	19	24	49	30	55	20
Ti	63	57	57	57	58	61	61	59	57
Mn	865	829	827	830	859	807	796	668	671
Fe	4140	3920	4110	4060	4520	4200	4100	4100	3810
Co (ppb)	136	78	126	121	133	371	275	166	359
Zn	91.0	92.7	98.0	122.8	108.2	49.5	58.7	67.9	42.6
Ga	34.4	34.5	35.8	34.6	34.7	33.4	35.7	35.8	34.2
As	40.8	50.4	54.6	27.8	18.7	6.0	8.4	23.2	1.0
Br	0.3	0.6	< 1	0.5	0.7	0.7	1.8	1.2	0.3
Rb	1933	1853	1831	1884	1807	1466	1527	1620	1329
Sr	97.7	183.0	221.0	70.8	177.0	127.0	89.6	14.4	24.5
Zr	26.8	17.7	17.3	20.3	17.8	22.4	17.8	15.1	21.1
Nb	85.0	82.3	84.6	81.1	82.1	86.8	81.7	80.5	79.5
Mo	1.5	0.9	0.5	0.9	2.4	1.5	2.9	1.6	1.2
Ag	0.2	< 0.8	0.7	< 0.8	0.2	< 0.6	< 0.5	< 0.6	0.3
Cd	0.3	0.3	0.3	0.4	0.3	0.3	0.3	< 0.1	0.2
Sn	502	487	476	489	480	518	488	497	493
Sb	2.05	2.52	2.47	1.55	3.65	1.58	1.29	0.65	0.82
Cs	362	376	319	303	207	341	516	367	282
Ba	35.9	58.1	57.0	46.2	92.0	19.0	12.6	23.1	36.5
La	1.37	1.00	0.45	0.57	1.13	5.65	2.74	2.03	2.49
Ce	2.66	2.42		0.78		17.0	7.00	3.29	4.41
Nd						12.3	5.7		
Sm (ppb)	309	204	101	95		1530	966	140	378
Eu (ppb)	55	29	10	5.5		591	342	28	60
Tb (ppb)	74	54	31	27		274	237	22	78
Yb (ppb)	257	195	144	101		1170	515	75	149
Lu (ppb)	41	37	24	14.2		194	85	14.6	20
Hf	2.59	1.69	1.58	1.83	1.65	1.97	1.47	1.08	1.60
Ta	81.7	77.8	79.4	76.9	79.1	83.7	77.2	76.4	77.5
W	54.6	64.7	82.8	114.0	42.0	18.3	26.5	23.7	12.9
Pb	18.1	9.0	9.4	8.9	10.0	9.9	9.2	33.0	6.1
Th	0.31	0.27	0.30	0.34	0.30	0.34	0.22	0.30	0.27
U	14.2	14.4	14.5	14.6	15.7	14.6	9.95	7.84	7.08
Zr/Hf	10.3	10.5	10.9	11.1	10.8	11.4	12.1	14.0	13.2
Nb/Ta	1.04	1.06	1.07	1.06	1.04	1.04	1.06	1.05	1.03
Eu/Eu^*	0.48	0.37	0.25	0.15		1.15	0.95	0.62	0.45
La/Yb_n	3.4	3.3	2.0	3.6		3.1	3.4	17.4	10.8

Note: Values in ppm unless noted.

Trace elements

Although not as evolved as the economically mineralized granites, the Richemont rhyolite hosts high contents of Li (3200 ppm), Rb (1800 ppm), Sn (490 ppm), Ta (79 ppm), and Nb (83 ppm). Some other ore-forming elements also reach high levels, such as Be (90 ppm) and W (79 ppm). The enrichments in Li, Rb, Sn, Ta, Nb, Be, and W, together with the lack of enrichment in elements such as Mo (1 ppm) and the low Nb/Ta ratio (1.05), classify the rhyolite as a rare-metal-element melt of the peraluminous class.

Trace-element abundances for the Richemont rhyolite are presented in Table 9. The concentration of magnesium and first-row transition elements is low to very low (Mg 59 ppm, Sc 22 ppb, Ti 58 ppm, Mn 840 ppm, Fe 4100 ppm, Co 120 ppb), in accordance with the absence of mafic minerals. Moreover, ratios

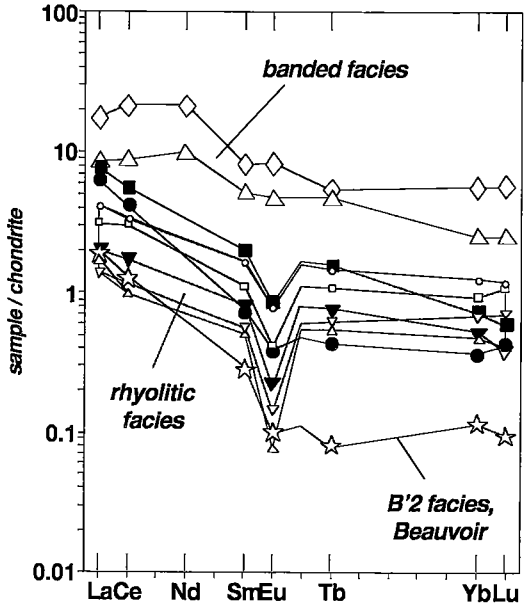

FIG. 9. *REE* patterns of the Richemont rhyolite, as compared with *REE* pattern of the B'2 facies of Beauvoir Ta–Li-enriched granite (open stars; Raimbault *et al.* 1995), which is otherwise similar to the Richemont rhyolite. Shaded symbols: banded facies, filled symbols: microcrystalline facies, small open symbols and shaded area: rhyolitic facies. The enriched pattern of the banded facies is unexplained, but is unlikely to be due to fractionation processes, since other elements (especially Ta) are at the same level as in the rhyolitic facies.

between elements attain quite unusual values when compared to those usually encountered in the crust (Taylor & McLennan 1985); for example, Fe/Mn is low (4.9 in Richemont rhyolite *versus* 58 in the crust), whereas Fe/Mg (69 *versus* 2.6), Fe/Ti (70 *versus* 12), Fe/Sc (1.8×10^6 *versus* 3200), and Fe/Co (3.4×10^5 *versus* 3500) are all very high.

Low contents of the *REE*, Zr, Hf, and Th are related to a low solubility of accessory minerals like zircon (Watson & Harrison 1983) or monazite (Rapp & Watson 1986, Montel 1986) in peraluminous melts. However, this fact alone cannot account for the low Zr/Hf value (10.7) or the moderate Eu anomaly (0.3). Moreover, the contents of Th, the bulk-rock *REE*, and the shape of the *REE* pattern (Fig. 9) differ from those of the B'2 facies in the Beauvoir granite, even though all other chemical parameters are similar. The differences between trace-element abundances in the B'2 facies of the Beauvoir granite and the Richemont dyke may reflect the effects of melting various source-rock lithologies, whereas the similarities in trace-element abundances between the two are more likely the result of fractional crystallization.

With the exception of the high fluorine contents, volatile elements do not seem to have been present at significant levels in the melt. Because of devitrification, the measured Cl content (14 ppm) does not reflect the initial contents. In addition, Cl was not detected in muscovite, whereas fluorine is abundant, leading to $X_F/X_{Cl} > 100$. This result points to the large predominance of F over Cl in the Richemont melt; evaluation of volatile fugacity ratios (Munoz 1984) yields log $[f(H_2O)/f(HF)] \approx 3.1$. Similarly, there are low contents of boron and sulfur (80 and 130 ppm, respectively).

The chalcophile elements Zn, As, Ag, Sb, and Cd are present at rather high levels, suggesting strongly that no loss of the vapor phase has occurred, those elements being trapped in glass or in vesicles already mentioned. These samples thus are considered to provide a good approximation of the rare-metal-bearing melt.

High Ga and Cs, moderate U, and low Ba and Pb contents are in agreement with the general characteristics of the rock. In contrast, high Sr contents (150 ppm), although unexpected in such a highly evolved environment and quite uncommon in ore-bearing granites, are similar to values found in the Beauvoir granite. In the latter case, the Sr isotope geochemistry shows unambiguously that such high values are of magmatic origin (Raimbault *et al.* 1995), emphasizing again that the Richemont rhyolite is a good approximation of a quenched rare-metal melt.

MELT EVOLUTION

Effect of mineral assemblage

The only mafic mineral in the assemblage of phenocrysts is a Li–Fe-bearing muscovite. Therefore, with the exception of a few elements like Sr, Ba, Rb, Pb, or Eu, which can be trapped in the two feldspars, geochemical evolution of melt is controlled by the crystallization of muscovite and accessory minerals. Owing to their subordinate character, accessory minerals will affect only their major constituent elements. The presence of uranium and tungsten niobates, in which Ta is a minor element only, explains quite well the differential behavior of ore elements Nb–Ta–W. In peraluminous granitic series, Ta increases much more rapidly than Nb, which in turn increases more quickly than W (Raimbault *et al.* 1987). However, it is known from the study of the Beauvoir complex (Raimbault *et al.* 1995) that Nb increases during the evolution of such melts, implying that Nb-bearing accessory phases become more soluble as evolution proceeds. This can be achieved by an increase in fluorine concentration. Experimental evidence suggests that an increase in F content promotes the solubility of columbite, tantalite, rutile, and zircon (Keppler 1993). This is in complete agreement with the absence of zircon, both as microphenocrysts and as inclusions in muscovite

TABLE 10. TRACE-ELEMENT DATA, MUSCOVITE SEPARATES, RICHEMONT DYKE, MASSIF CENTRAL, FRANCE

Sample		L14d			L14c3			L14e2	
Anal.#	icp	66	67	68	69	70	71	72	73
m, μg		124.9	70.2	62.5	70.5	41.1	93.5	47.6	47.6
FeO %	5.16	5.0	4.75	4.54	4.48	4.97	4.63	4.99	6.57
Li	2033								
Be	21.0								
Mg	507								
Sc	1.22		1.19	0.83	1.20	1.09	0.99	1.54	1.39
Ti	1090								
Mn	1690								
Co			< 1.3	< 1.1	3.7	6.2	3.0	10.6	7.8
Zn	617	627	655	598	528	642	609	584	722
As		< 12	32.5	1.6	167	33.5	2.0	1.8	< 1.2
Rb		3814	4211	4050	4024	4139	4247	4058	4707
Sr	19.4#								
Nb	287								
Sn		-	176	157	165	169	170	191	202
Sb		1.7	3.59	< 0.13	0.30	0.23	0.47	< 0.24	< 0.2
Cs		157	124	132	128	140	187	124	174
Ta		33.0	30.3	32.3	39.1	35.9	32.7	31.1	56.8
W		82	110	101	172	139	105	108	118
U		< 3	0.59	0.80	1.53	1.02	0.51	0.47	2.95
Partition coefficients									
Li	0.59								
Be	0.24								
Mg	11.3								
Sc	50.8		49.6	34.6	57.1	51.9	47.1	51.3	46.3
Ti	18.8								
Mn	1.97								
Fe	8.87	8.59	8.16	7.80	8.47	9.40	8.75	9.45	12.4
Co			< 9.77	< 8.27	29.4	49.2	23.8	38.5	28.4
Zn	5.70	5.79	6.05	5.53	5.39	6.55	6.21	9.95	12.3
Rb		2.11	2.33	2.24	2.20	2.26	2.32	2.66	3.08
Nb	3.5								
Sn			0.37	0.33	0.35	0.36	0.36	0.39	0.41
Cs		0.76	0.60	0.64	0.40	0.44	0.59	0.24	0.34
Ta		0.42	0.38	0.41	0.49	0.45	0.41	0.40	*
W		1.95	2.62	2.40	2.08	1.68	1.27	*	*
U			0.04	0.05	0.11	0.07	0.04	0.05	*

Compositions are reported in ppm, except for FeO, in weight %. Samples L14d and L14c3: rhyolitic facies; sample L14e: banded facies. All analyses were made with IENAA of individual phenocrysts (*m* is the mass), except bulk fraction "icp" of sample L14d, analyzed by ICP-AE.

* No partition coefficient was derived because of suspected contamination by accessory minerals. This is also the case for As and Sb.

\# Although the isotopic composition of Sr was not determined, the Sr contents of muscovite may be attributed to the *in situ* decay of ^{87}Rb since 300 million years.

phenocrysts, the increase of Ti content in niobates during crystallization, and the evolution of Nb/Ta in those niobates. Cassiterite is also soluble in the Richemont melt, in accordance with experimental data (Štemprok 1990). The lack of apatite phenocrysts is also well explained by experimental results showing an enhanced solubility of phosphorus in peraluminous melts (Pichavant *et al.* 1992).

Partition coefficients for muscovite

Analyses of single crystals of muscovite (Table 10) can be used to assess the effect of muscovite crystallization on melt evolution. Experimentally determined muscovite – melt partition coefficients for Li, Rb, Cs, and F (Icenhower & London 1995) match very closely muscovite – rock values measured in the Richemont rhyolite. This match argues strongly for the interpretation of muscovite as phenocrysts and, therefore, for the use of crystal:rock ratios as reliable proxies for true muscovite – melt partition coefficients. Partition coefficients are low for Cs (0.4–0.6), Li (0.6), Be (0.24), Ta (0.42 ± 0.04), Sn (0.37 ± 0.03), and U (0.06 ± 0.03). With the exception of Ta and U, the behavior of which is also dependent on accessory phases, these elements must increase during evolution. For Rb, partition coefficients are greater than one (2.24 ± 0.08), but a low modal amount (by volume) of muscovite (0.1) and a low Rb partition coefficient for albite (0.2) explains why Rb still increases in such melts. For W and Nb, partition coefficients for muscovite are greater than unity (1.3–2.6 and 3.5, respectively), and these elements are not partitioned into the feldspar assemblage, so their behavior mimics

that of Rb. However, the difference between partition coefficients of Nb (3.5) and Ta (0.42) in muscovite can easily account for the observed behavior of these elements (Ta increasing more than Nb) in peraluminous granites (Raimbault *et al.* 1987), even where no accessory W–Nb-bearing phase occurs. Finally, the behavior of first-row transition elements is easily explained by the decrease of measured muscovite – melt partition coefficients in the order Sc (48 ± 7), Fe (8.5 ± 0.6), Zn (5.9 ± 0.5), and Mn (2.0), leading to very high Fe/Sc, and low Fe/Mn and Fe/Zn values in the melt. Partition coefficients for Mg (approximately 11) do not explain the very low Mg content in the Richemont rhyolite, but it should be emphasized that no variation in Mg is observed in the various units of the Beauvoir granite (Raimbault *et al.* 1995). Fractionation involving Fe and Mg is more easily explained by an earlier stage involving biotite, since incorporation of fluorine promotes the trapping of Mg relative to Fe due to F–Fe avoidance (Munoz 1984).

Microcrystalline Facies and their Interpretation

Petrography

The nature and relative amounts of phenocrysts are identical in crystalline and rhyolitic facies. The only difference is the presence of a thin border on phenocrysts in the microcrystalline facies, whereas phenocrysts in rhyolitic facies have a sharp contact with the matrix. Compositions of muscovite borders in the microcrystalline facies show a larger content of the muscovite end-member, and follow the same trends as phenocrystic muscovite, with the exception of lower Na content. The minerals in the groundmass, *i.e.*, quartz, mica, albite and microcline, are identical to those in the groundmass of the rhyolitic facies. However, the texture is aplitic, with a uniform size of crystals, very different from the devitrified texture of the rhyolitic facies. The texture of the microcrystalline facies suggests that the remaining melt crystallized more slowly than in the rhyolitic facies. As a consequence of this "slow" crystallization, dissolved H_2O may well have had time to escape as a hydrothermal fluid. The composition of the resulting rock must therefore be considered to be affected by escape of fluid from a melt, the composition of which is indicated by the rhyolitic facies. The Richemont dyke provides thus a unique chance to study the effect of fluid–melt interaction in natural systems.

Geochemistry

The major-element composition of the microcrystalline facies is shifted toward higher silica and lower Na/K atomic ratio relative to the rhyolitic facies. This result is not in agreement with fluid–melt partitioning experiments (London *et al.* 1988), which suggest that the melt dissolves congruently in the vapor phase, leading to identical Na–K–Si–Al relationships in the melt and in the residue. However, the experimental evidence is based on systems that are not as enriched in F as the Richemont rhyolite. At Richemont, F contents of the microcrystalline facies are less than half those of the rhyolitic facies, showing the preference of fluorine for the fluid, in agreement with experimental data of Webster (1990) for very F-rich systems. Higher F content in the fluid phase should therefore enhance the solubility of albite over that of quartz and K-feldspar, leading to a residue shifted away from the albite corner compared to the composition of the rhyolite facies as projected in the haplogranite system.

Modeling of the fluid phase

Considering that the microcrystalline facies represents the residue after separation of a fluid phase, it is possible to estimate the vapor – melt partition coefficients D. If D does not vary and is fixed at a constant D_0 value during exchange, the ratio of concentration c^* in the residue to concentration c_0 in the melt is given by

$$\ln (c^*/c_0) = (D_0 - 1) \bullet \ln (1 - h), \quad (1)$$

where h is the concentration of H_2O in the melt. If, as it is probable, D is not constant, but decreases (or increases), the true concentration in the residue is higher (or lower) than the calculated c^* value. An approximate value of the partition coefficient D_0 at the beginning of the distillation process may be estimated from equation (1) using the measured value of c^*/c_0 (Fig. 10).

Phosphorus is one of the most depleted elements in the microcrystalline facies, relative to the rhyolitic facies. However, Keppler (1994) has shown experimentally that phosphorus is fractionated in favor of the melt at low pressures. These contradictory results can be reconciled, however, since fluid unmixing postdates the formation of the phosphate aggregates, as shown by the absence of evidence for fluid unmixing in the rhyolitic facies. Under such conditions, the extreme depletion of phosphorus in the microcrystalline facies could be due to leaching of phosphate aggregates already formed by very acid fluorine-rich fluids that subsequently unmixed from the silicate–melt part of the system. Such a scenario is strongly supported by the absence of phosphate aggregates in the microcrystalline facies. As a consequence, depletion data for P, and the Ca and Sr associated with P in phosphates, cannot be interpreted in terms of equilibrium partition-coefficients; instead, their abundance is controlled by their late-stage removal from the microcrystalline facies.

Also, the behavior of Mg, Sc, Co, and Cl cannot be explained by this model. The first three elements are extremely depleted in the initial melt, and even a very

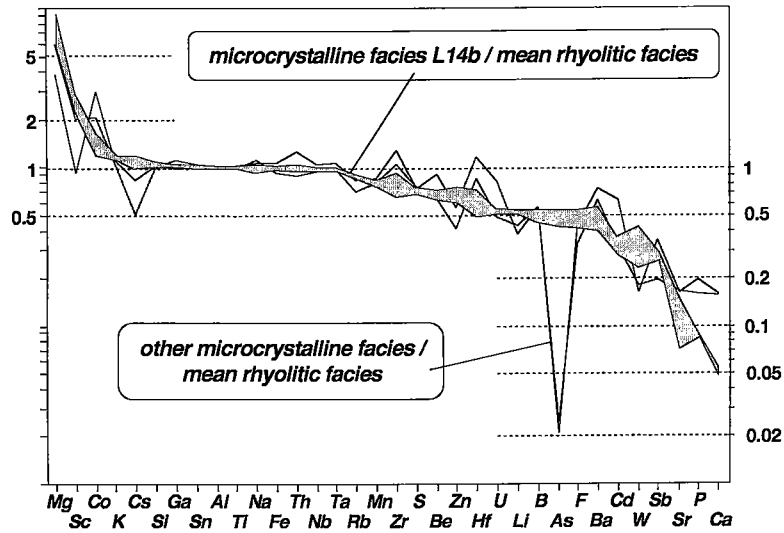

FIG. 10. Ratios of contents of various elements in the microcrystalline facies to contents in the rhyolitic facies (c/c_0), arranged in order of increasing depletion. The range of variation is highlighted for sample L14b of the microcrystalline facies; mean lines only are given for other samples. In the case of Zr and Hf, heterogeneity of zircon distribution may account for the observed differences. See text for further details.

small influence attributable to the host rocks (especially amphibolites) can account for the observed enrichment in the residual rock. Chlorine depletion in the rhyolitic facies is assigned to late devitrification, which did not occur in the microcrystalline facies. The residual Cl value for the microcrystalline phase after fluid unmixing may therefore be used to estimate an initial value for the melt in the range of 60–130 ppm, on the basis of published vapor – melt partition coefficients (Webster & Holloway 1990, Webster 1992). Although this value is probably underestimated owing to Cl loss from the microcrystalline facies under subsurface conditions, it points out the extreme predominance of fluorine over chlorine in these peraluminous systems.

Partition coefficients of elements for which the ratio c^*/c_0 is close to 1 cannot be calculated accurately without a very precise estimation of h, the initial content of H_2O. The only elements for which D_0 is significantly greater than 1 (*i.e.*, concentrated in the melt) are Si, Ga, and K. For Sn, Al, Ti, Na, Fe, Th, Nb, and Ta, the values are too close to unity to be conclusive. Moreover, a small input of Si and K from the surrounding rocks cannot be excluded, since such an exchange is evident, at least at a low level, in the distribution of Mg, Sc, and Co. This would result in a dilution of the other elements, leading to slightly depleted values of c^*/c_0. It is noteworthy that Sn does not seem to have been fractionated in the fluid, suggesting a high fugacity of oxygen.

For elements distinctly depleted in the microcrystalline facies, approximate values of the fluid–melt partition coefficients may be computed, although such estimates are strongly dependent on h, the initial content of H_2O. A value $h = 0.10$ has been chosen for modeling purposes (Webster 1990, London *et al.* 1988). As a result of the numerous assumptions, precise values are meaningless, and we present here qualitative results only. Resulting values of D_0 deduced from equation (1) cluster as follows: 2–3 for Rb and Mn, 4–5 for S, Be, and Zn, 7–8 for U, Li, B, As, F, and Ba, and 12–13 for W and Sb. Values in the range 23–30 for Sr, P, and Ca cannot be considered as partition coefficients (see above); the values indicate, however, that these elements will be removed from the system if a F-rich fluid is exsolved.

Some elements (Zr, Hf, and the *REE*) are controlled by scarce accessory phases and cannot therefore be used in such calculations, because concentration ranges in the rhyolitic and microcrystalline facies largely overlap. Nevertheless, it appears that differential behavior does occur within these families, with an increase in the Zr/Hf and La/Lu values from rhyolitic facies to microcrystalline facies, indicating that Hf and *HREE* are more easily transported by fluids than are Zr and La. For the *REE* at least, this result is not concordant with experimental data in Cl-rich systems, according to which vapor – melt partition coefficients favor *LREE* incorporation in the fluid (Flynn & Burnham 1978).

Mass-balance calculations have been performed so that the mean composition of the hydrothermal solution can be estimated. Convergence was achieved for $h = 0.029$ (*i.e.*, 2.9 wt%). Results, however, are not internally consistent, since values for K would be negative. This is interpreted as resulting from late mobility of K and possibly Si during cooling. The influx of K easily accounts for the alteration of plagioclase to mica. Some late silicification could also have occurred, yielding a systematic bias in the calculations. Analytical uncertainties for major elements, especially Si, also yield scattered results, because even good determinations of Si (typically with less than 1% relative uncertainty) lead to large ranges in absolute error (as compared to other elements). Nevertheless, some qualitative conclusions can be drawn as follows: 1) The amount of dissolved silicate in the fluid is quite high, about 1/3 (*i.e.*, 30 wt%), in qualitative agreement with experimental data (London *et al.* 1988). 2) The concentration of F also is large, perhaps as high as 20%; in comparison, hydrous melts with striking Cl contents have been observed in highly evolved peralkaline magmas by Lowenstern (1994), also in agreement with experimental data on the behavior of Cl in felsic melt – H_2O systems (Kravchuk & Keppler 1994). 3) Major elements in the solute are Si, Al, Na, Ca, and include Li. The behavior of K cannot be assessed. 4) The minor elements (in the range 0.1 to 1%) in the solute include Mn, Fe, Zn, Rb, Sr, and W, and possibly S and Cl. 5) The Fe/Mn ratio is about 1 in the fluid *versus* 5 in the melt.

Conclusions

A petrographic analysis of the Richemont dyke points out the quenched-melt character of the rock, with very restricted subsolidus recrystallization, limited to devitrification of the matrix. The chemical composition of the rhyolitic rocks provides evidence that the melt belongs to the group of rare-metal-enriched pegmatite-forming magmas specifically related to the Ta–Li–Sn-mineralized Beauvoir granite.

There are, however, striking mineralogical differences between the rare-metal granites of the Beauvoir family and the quenched magmatic assemblages of the Richemont rhyolite. Such differences, pertaining to the nature of phenocrysts (absence of topaz, muscovite instead of lepidolite and "wolframo-ixiolite" instead of columbite – tantalite), suggest that the mineral assemblages observed in granites are related to the ultimate stages of magmatic evolution, commonly in the presence of a fluid phase. Earlier-formed magmatic crystals, which are preserved in the Richemont rhyolite, re-equilibrated during these later stages of magmatic evolution. Such crystals may therefore be missed in granites, where they possibly occur only as tiny relics.

Inferred muscovite – melt partition coefficients measured in phenocrysts agree much more closely than do mineral assemblages of rare-metal granites with respect to the known evolution of rare-metal-enriched melts, as exemplified by Li, which has a low partition-coefficient and is therefore expected to increase, as observed. Minerals observed in rare-metal granites are unlikely to constrain efficiently models of evolution in rare-metal-enriched melts.

Finally, the effect of fluid unmixing may be assessed using the microcrystalline facies of the dyke. The observed patterns of depletion are admittedly probably the result of complex relations involving more than two phases, but they provide conservative estimates for the behavior of a large series of elements that do not seem to be quantitatively removed from the melt at this stage. This includes a large set of elements, covering many geochemical groups: Ga and the major elements Si and Al, high-field-strength elements Nb, Ta, Th, Ti, Zr, Hf, and Sn, Mg, Fe and Co, the rare-earth elements, including Sc, and even the alkali elements Na, K, Rb, and Cs. For such elements, the use of bulk-rock granite compositions as a proxy for melt composition is therefore justified by this study.

Acknowledgements

Support for this research was provided by the Commission of European Communities under grant number MSM040F, by ATP "Métallogénie" of the CNRS, and by funds of the Ecole des Mines de Paris. A first version of this manuscript was substantially improved by helpful comments by Miroslav Štemprok. The readability of the final version owes much to careful reviews by Karen Webber, Al Falster, and Skip Simmons.

References

Antipin, V.S., Gayvoronskii, B.A., Sapozhnikov, V.P. & Pisarskaya, V.A. (1980): Ongonites from the Sherlovaia Gora area (eastern Transbaykalia). *Dokl. Akad. Nauk SSSR* **253**, 228-232 (in Russ.).

Aubert, G. (1969): Les coupoles granitiques de Montebras et d'Echassières (Massif Central Français) et la genèse de leur minéralisation en étain, tungstène, lithium et béryllium. *Bureau de Recherches Géologiques et Minières, Mém.* **46**.

Aurisicchio, C., Orlandi, P., Pasero, M. & Perchiazzi, N. (1993): Uranopolycrase, the uranium-dominant analogue of polycrase-(Y), a new mineral from Elba Island, Italy, and its crystal structure. *Eur. J. Mineral.* **5**, 1161-1165.

Barton, M.D. & Frantz, J.D. (1983): Exchange equilibria of alkali feldspars with fluoride-bearing fluids. *Carnegie Inst. Wash., Yearbook* **82**, 377-381.

BOTTINGA, Y. & JAVOY, M. (1975): Oxygen isotope partitioning among the minerals in igneous and metamorphic rocks. *Rev. Geophys. Space Phys.* **13**, 401-418.

BURNOL, L. (1974): Géochimie du béryllium et types de concentration dans les leucogranites du Massif Central français; relations entre les caractéristiques géochimiques des granitoïdes et les gisements endogènes de type départ acide (Be, Sn, Li) ou de remaniement tardif (U, F, Pb et Zn). *Bureau de Recherches Géologiques et Minières, Mém.* **85**.

ČERNÝ, P. (1992): Geochemical and petrogenetic features of mineralization in rare-element granitic pegmatites in the light of current research. *Applied Geochem.* **7**, 393-416.

_____ & ERCIT, T.S. (1989): Mineralogy of niobium and tantalum: crystal chemical relationships, paragenetic aspects and their economic implications. *In* Lanthanides, Tantalum and Niobium (P. Möller, P.Černý & F. Saupé, eds.). Springer Verlag, Berlin, Germany (27-79).

_____, _____ & WISE, M.A. (1992): The tantalite – tapiolite gap: natural assemblages versus experimental data. *Can. Mineral.* **30**, 587-596.

CHEILLETZ, A., ARCHIBALD, D.A., CUNEY, M. & CHAROY, B. (1992): Ages $^{40}Ar/^{39}Ar$ du leucogranite à topaze–lépidolite de Beauvoir et des pegmatites sodolithiques de Chèdeville (Nord du Massif Central, France). Signification pétrologique et géodynamique. *C.R. Acad. Sci. Paris, Sér.* **II, 315**, 329-336.

CONGDON, R.D. & NASH, W.P. (1991): Eruptive pegmatite magma: rhyolite of the Honeycomb Hills, Utah. *Am. Mineral.* **76**, 1261-1278.

DINGWELL, D.B., SCARFE, C.M. & CRONIN, D.J. (1985): The effect of fluorine on viscosities in the system Na_2O – Al_2O_3 – SiO_2: implications for phonolites, trachytes and rhyolites. *Am. Mineral.* **70**, 80-87.

DU BRAY, E.A. (1994): Compositions of micas in peraluminous granitoids of the eastern Arabian Shield – implications for petrogenesis and tectonic setting of highly evolved, rare-metal enriched granites. *Contrib. Mineral. Petrol.* **116**, 381-397.

DUTHOU, J.L. (1977): Chronologie Rb–Sr et géochimie des granitoïdes d'un segment de la chaîne varisque, relations avec le métamorphisme: le Nord Limousin. *Annales Scientifiques de l'Université de Clermont* **63**, 1-294.

FLYNN, R.T. & BURNHAM, C.W. (1978): An experimental determination of rare earth partition coefficients between a chloride-containing vapor phase and silicate melts. *Geochim. Cosmochim. Acta* **42**, 685-701.

FOUILLAC, A.M. & ROSSI, P. (1991): Near-solidus ^{18}O depletion in a Ta–Nb-bearing albite granite: the Beauvoir granite, France. *Econ. Geol.* **86**, 1704-1720.

GINZBURG, A.I., GORZHEVSKAYA, S.A., SIDORENKO, G.A. & UKHINA, T.A. (1969): Wolframoixiolite, a new variety of ixiolite. *Zap. Vses. Mineral. Obshchest.* **98**, 63-73 (in Russ.).

GRAMENITSKY, E.N. & SHCHEKINA, T.I. (1993): Phase relations in the liquidus part of the fluorine-bearing granite system. *Geokhimiya* **6**, 821-841 (in Russ.).

GREEN, N.L. & USDANSKY, S.I. (1986): Toward a practical plagioclase – muscovite thermometer. *Am. Mineral.* **71**, 1109-1117.

ICENHOWER, J. & LONDON, D. (1995): An experimental study of element partitioning among biotite, muscovite, and coexisting peraluminous silicic melt at 200 MPa (H_2O). *Am. Mineral.* **80**, 1229-1251.

KEPPLER, H. (1993): Influence of fluorine on the enrichment of high field strength trace elements in granitic rocks. *Contrib. Mineral. Petrol.* **114**, 479-488.

_____ (1994): Partitioning of phosphorus between melt and fluid in the system haplogranite – H_2O – P_2O_5. *Chem. Geol.* **117**, 345-353.

KOVALENKO, V.I. & KOVALENKO, N.I. (1976): *Ongonites (Topaz-Bearing Quartz Keratophyre) – Subvolcanic Analogues of Rare-Metal Li–F Granites*. Nauka, Moscow, Russia (in Russ.).

KRAVCHUK, I.F. & KEPPLER, H. (1994): Distribution of chloride between aqueous fluids and felsic melts at 2 kbar and 800°C. *Eur. J. Mineral.* **6**, 913-923.

LONDON, D., HERVIG, R.L. & MORGAN, G.B. VI (1988): Melt–vapor solubilities and elemental partitioning in peraluminous granite – pegmatite systems: experimental results with Macusani glass at 200 MPa. *Contrib. Mineral. Petrol.* **99**, 360-373.

LOWENSTERN, J.B. (1994): Chlorine, fluid immiscibility and degassing in peralkaline magmas from Pantelleria, Italy. *Am. Mineral.* **79**, 353-369.

MANNING, D.A.C. (1981): The effect of fluorine on liquidus phase relationships in the system Qz–Ab–Or with excess water at 1 kb. *Contrib. Mineral. Petrol.* **76**, 206-215.

MONTEL, J.-M. (1986): Experimental determination of the solubility of Ce-monazite in SiO_2 – Al_2O_3 – K_2O – Na_2O melts at 800°C, 2 kbar, under H_2O-saturated conditions. *Geology* **14**, 659-662.

MUNOZ, J.L. (1984): F–OH and Cl–OH exchange in micas with applications to hydrothermal ore deposits. *In* Micas (S.W. Bailey, ed.). *Rev. Mineral.* **13**, 469-493.

MYSEN, B.O., RYERSON, F.J. & VIRGO, D. (1981a): The structural role of phosphorus in silicate melts. *Am. Mineral.* **66**, 106-117.

_____ & VIRGO, D. (1985): Structure and properties of fluorine-bearing aluminosilicate melts: the system Na_2O – Al_2O_3 – SiO_2 – F at 1 atm. *Contrib. Mineral. Petrol.* **91**, 205-220.

_____, _____ & KUSHIRO, I. (1981b): The structural role of aluminum in silicate melts – a Raman spectroscopic study at 1 atmosphere. *Am. Mineral.* **66**, 678-701.

_____, _____ & SEIFERT, F.A. (1985): Relationships between properties and structure of aluminosilicate melts. *Am. Mineral.* **70**, 88-105.

PICHAVANT, M., BOHER, M., STENGER, J.F., AISSA, M. & CHAROY, B. (1987): Relations de phase des granites de Beauvoir à 1 et 3 kbar en conditions de saturation en H_2O. *In* Le forage scientifique d'Echassières (M. Cuney & A. Autran, eds.). *Géologie de la France* **2-3**, 77-86.

_____, MONTEL, J.-M. & RICHARD, L.R. (1992): Apatite solubility in peraluminous liquids: experimental data and an extension of the Harrison–Watson model. *Geochim. Cosmochim. Acta* **56**, 3855-3861.

RAIMBAULT, L. & AZENCOTT, C. (1987): Géochimie des éléments majeurs et traces du granite à métaux rares de Beauvoir (sondage GPF, Echassières). *In* Le forage scientifique d'Echassières (M. Cuney & A. Autran, eds.). *Géologie de la France* **2-3**, 189-198.

_____, CHAROY, B., CUNEY, M. & POLLARD, P.J. (1991): Comparative geochemistry of Ta-bearing granites. *In* Source, Transport and Deposition of Metals (M. Pagel & J. Leroy, eds.). Balkema, Rotterdam, The Netherlands (793-796).

_____, CUNEY, M., AZENCOTT, C., DUTHOU, J.-L. & JORON, J.-L. (1995): Geochemical evidence for a multistage magmatic genesis of Ta–Sn–Li mineralization in the granite at Beauvoir, French Massif Central. *Econ. Geol.* **90**, 548-576.

_____, MEYER, G. & TREUIL, M. (1987): Comportements différenciés de W, Sn, U, Ta, Nb dans quelques complexes granitiques du Massif Central Français. *Bull. Minéral.* **110**, 591-601.

RAMSDEN, A.R., FRENCH, D.H. & CHALMERS, D.I. (1993): Volcanic-hosted rare-metal deposit at Brockman, Western Australia – mineralogy and geochemistry of the Niobium Tuff. *Mineral. Deposita* **28**, 1-12.

RAPP, R.P. & WATSON, E.B. (1986): Monazite solubility and dissolution kinetics: implications for the thorium and light rare earth chemistry of felsic magmas. *Contrib. Mineral. Petrol.* **94**, 304-316.

SCHLEICHER, H. & LIPPOLT, H.J. (1981): Magmatic muscovite in felsitic parts of rhyolites from southwest Germany. *Contrib. Mineral. Petrol.* **78**, 220-224.

ŠTEMPROK, M. (1990): Solubility of tin, tungsten and molybdenum oxides in felsic magmas. *Mineral. Deposita* **25**, 205-212.

STORMER, J.C., JR. (1975): A practical two-feldspar geothermometer. *Am. Mineral.* **60**, 667-674.

SUWIMONPRECHA, P., ČERNÝ, P. & FRIEDRICH, G. (1995): Rare metal mineralization related to granites and pegmatites, Phuket, Thailand. *Econ. Geol.* **90**, 603-615.

TAYLOR, S.R. & MCLENNAN, S.M. (1985): *The Continental Crust: its Composition and Evolution.* Blackwell, Boston, Massachusetts.

TUTTLE, O.F. & BOWEN, N.L. (1958): Origin of granite in the light of experimental studies in the system $NaAlSi_3O_8$ – $KAlSi_3O_8$ – SiO_2 – H_2O. *Geol. Soc. Am., Mem.* **74**.

WATSON, E.B. & HARRISON, T.M. (1983): Zircon saturation revisited: temperature and composition effects in a variety of crustal magma types. *Earth Planet. Sci. Lett.* **64**, 295-304.

WEBSTER, J.D. (1990): Partitioning of F between H_2O and CO_2 fluids and topaz rhyolite melt: implications for mineralizing magmatic–hydrothermal fluids in F-rich granitic systems. *Contrib. Mineral. Petrol.* **104**, 424-438.

_____ (1992): Water solubility and chlorine partitioning in Cl-rich granitic systems: effects of melt composition at 2 kbar and 800°C. *Geochim. Cosmochim. Acta* **56**, 679-687.

_____ & HOLLOWAY, J.R. (1990): Partitioning of F and Cl between magmatic hydrothermal fluids and highly evolved granitic magmas. *Geol. Soc. Am., Spec. Pap.* **246**, 21-34.

Received August 15, 1997, revised manuscript accepted March 7, 1998.